ChemComm

COMMUNICATION

View Article Online
View Journal | View Issue

Cite this: *Chem. Commun.*, 2023, **59**, 4974

Received 1st February 2023,
Accepted 23rd March 2023

DOI: 10.1039/d3cc00460k

rsc.li/chemcomm

Creation of single molecular conjugates of metal–organic cages and DNA†

Toshinobu Nakajo,[a] Shinpei Kusaka,[a] Haruka Hiraoka,[b] Kohei Nomura,[b] Noriaki Matsubara,[b] Rintaro Baba,[b] Yuki Yoshida,[b] Kosuke Nakamoto,[b] Masakazu Honma,[c] Hiroaki Iguchi,[a] Takayuki Uchihashi,[de] Hiroshi Abe[be] and Ryotaro Matsuda*[a]

Here we report the development of an equimolar conjugate of a metal–organic cage (MOC) and DNA (MOC-DNA). Several MOC-DNA conjugates were assembled into a programmed structure by coordinating with a template DNA having a complementary base sequence. Moreover, conjugation with the MOC drastically enhanced the permeability of DNA through the lipid bilayer, presenting great potential as a drug delivery system.

Nanoporous metal complexes (NPMCs) are solid materials with nanometer-sized pores constructed by the self-assembly of metal ions and organic ligands.[1] NPMCs can accommodate small molecules in their pores, and thus have been investigated for applications such as selective adsorbents,[2,3] reaction catalysts,[4–6] and drug delivery vehicles.[7,8] Moreover, the outer surface of the framework can be further functionalized through a post-synthetic modification, conferring additional properties like processability and dispersity.[9,10]

Recently, the conjugation of metal–organic frameworks (MOFs), a class of NPMCs with an infinite structure, and DNA has attracted much interest. Since DNA has biological functions based on its sequences, MOF–DNA conjugates have been investigated not only for engineering applications such as aptasensors[11] and immunoassays,[12] but also as *in vivo* drug delivery systems (DDSs). For example, MOFs modified with DNA on their surfaces can effectively transport DNA into cells, or control the release of proteins and drugs from the pores.[13,14] Moreover, exploiting its complementary base pair coordination, DNA can be used to fabricate nano- and micro-structures such as DNA origami.[15] Similarly, ordered MOF assemblies have been obtained by modifying DNA on the particle surface.[16,17] In general, these MOF–DNA conjugates are non-stoichiometric due to the infinite structure of MOFs, which would be unsuitable for the precise molecular design of NPMC assemblies or as DDSs.

Metal–organic cages (MOCs) are NPMCs with discrete structures. In contrast to MOFs, MOCs are soluble in various solvents and their surface can be modified quantitatively, enabling the precisely controlled design of MOC-organic molecule conjugates at the molecular level.[18] Such a structural feature is also expected in conjugating DNA and MOCs, which is advantageous for the precise molecular design of NPMC assemblies or DDSs in aqueous solution (Fig. 1). However, conjugation of DNA and MOCs has not been reported, presumably because DNA is more difficult to conjugate with MOCs than with MOFs because of multiple coordination sites of DNA: MOCs decompose even if one metal ion is subtracted, while MOFs retain their properties even when part of their surface is damaged.

In this study, we achieved stoichiometric conjugation of DNA with a specially designed new MOC through a post-synthetic modification. Modifying DNA with MOCs has enabled the design of MOC assemblies by forming a double-strand DNA and has significantly improved the affinity of DNA toward human cells.

Due to its water stability and ease of post-synthetic surface modifications, we selected Zr-MOC, having a trinuclear Zr

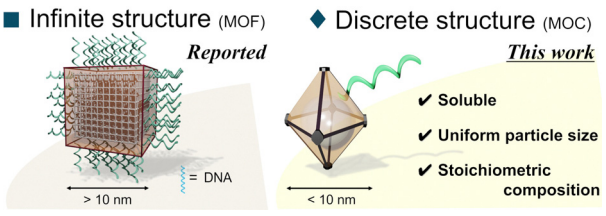

Fig. 1 Characteristics of discrete-NPMC decorated with DNA.

[a] *Department of Chemistry and Biotechnology, School of Engineering, Nagoya University, Furo-cho, Chikusa-ku, Nagoya 464-8603, Japan. E-mail: ryotaro.matsuda@chembio.nagoya-u.ac.jp*
[b] *Department of Chemistry, School of Science, Nagoya University, Chikusa-ku, Nagoya 464-8602, Japan*
[c] *Modality Research Laboratories 1, Research Unit, R&D Division, Kyowa Kirin Co., Ltd., Asahi-machi, Machida-shi, Tokyo 194-8533, Japan*
[d] *Department of Physics, School of Science, Nagoya University, Chikusa-ku, Nagoya 464-8602, Japan*
[e] *Institute for Glyco-core Research (iGCORE), Nagoya University, Chikusa-ku, Nagoya 464-8602, Japan*

† Electronic supplementary information (ESI) available: Experimental details, CCDC 2212480 (**MOC-2**) and 2190157 (**MOC-3**). For ESI and crystallographic data in CIF or other electronic format see DOI: https://doi.org/10.1039/d3cc00460k

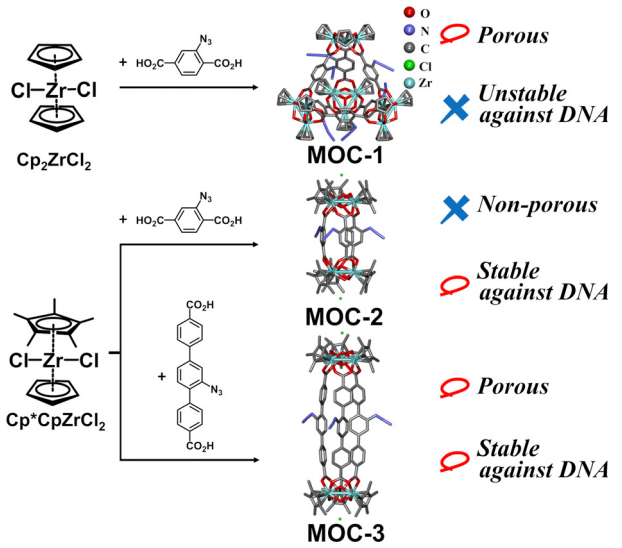

Fig. 2 Synthesis and crystal structure of each MOC. Because azide groups in **MOC-1** were severely disordered, the image of **MOC-1** was generated by adding azide groups manually to the obtained tetrahedral framework. The images of **MOC-2** and **MOC-3** are structures revealed by single-crystal X-ray structure analysis.

cluster capped by cyclopentadienyl (Cp) groups,[19] and modified it by introducing azide groups for the click reaction with terminal alkyne-containing DNA (see the ESI† and Fig. S1–S3 for the syntheses of MOC ligands and DNAs). Accordingly, we synthesized a new MOC, **MOC-1** [{$Cp_3Zr_3(\mu_3\text{-}O)(\mu\text{-}OH)_3$}$_4$-($\mu$-**BDC-N$_3$**)$_6$]$Cl_4$, with a tetrahedral cage from Cp_2ZrCl_2 and azide terephthalic acid (H_2**BDC-N$_3$**) (Fig. 2). The structure was revealed by single-crystal X-ray diffraction (SXRD) analysis, electrospray ionization mass spectrometry (ESI-MS), and infrared spectroscopy (Fig. S4–S6, ESI†). Next, its stability against DNA was evaluated. **MOC-1** and **Hexynyl-DNA** (Fig. 3a and Table S1, ESI†) were mixed in 50% acetonitrile/H_2O and incubated overnight. The ESI-MS spectrum of the resulting solution showed no peak derived from **MOC-1** (Fig. S7, ESI†), suggesting that DNA collapsed **MOC-1**, probably because DNA coordinates with the Zr ions as observed when UiO-66 was treated with DNA.[16]

To improve the stability of Zr-MOC, we changed the capping ligand from Cp to pentamethylcyclopentadienyl (Cp*) because stronger bonds and steric hindrance between Cp* and Zr are expected to stabilize the Zr cluster.

Then, we synthesized a new MOC, **MOC-2** [{$Cp^*_3Zr_3(\mu_3\text{-}O)$-($\mu$-OH)$_3$}$_2$($\mu$-**BDC-N$_3$**)$_3$]$Cl_2$, from Cp*CpZrCl$_2$ and H_2**BDC-N$_3$** (Fig. 2 and Fig. S8, ESI†). SXRD analysis and ESI-MS spectral measurements revealed that **MOC-2** had a cocoon-shaped structure with two Zr clusters bridged by three ligands. As **MOC-2** did not have internal pores (*i.e.*, it was not an NPMC), **MOC-3** [{$Cp^*_3Zr_3(\mu_3\text{-}O)(\mu\text{-}OH)_3$}$_2$($\mu$-**TDC-N$_3$**)$_3$]$Cl_2$ was synthesized with a longer ligand (azide-terphenyl dicarboxylate, H_2**TDC-N$_3$**). SXRD analysis and ESI-MS spectral measurements revealed that **MOC-3** was also cocoon-shaped (Fig. 2, Fig. S9 and S10, ESI†), but we confirmed the permanent porosity of **MOC-3** by an N_2 adsorption experiment (Fig. S11, ESI†).

Upon testing its stability against DNA in the same way as for **MOC-1**, the peaks derived from **MOC-3** were observed in the ESI-MS spectra and the peak intensity was comparable to that of the control (the sample that was not treated with **Hexynyl-DNA**, see Fig. S12, ESI†), indicating that **MOC-3** was stable against DNA. As expected, MOC showed improved stability against DNA by changing the capping site.

Since the copper-catalyzed click reaction between **MOC-3** and **Hexynyl-DNA** did not work well (see ESI,† Fig. S13 and S14), we synthesized **DBCO-DNA** having the dibenzocyclooctyne (DBCO) moiety, which is capable of a catalyst-free click reaction with an azide group, in the same base sequence as in **Hexynyl-DNA** (Fig. 3a and Table S1, ESI†). **MOC-3** and **DBCO-DNA** were heated in a 1 : 1 DEF/H_2O solution at 40 °C for about 24 h, diluted with water, filtered through a membrane filter, and analysed by reverse phase high-performance liquid chromatography (HPLC). A new peak was observed after 60 min of elution (Fig. 3b and see Fig. S15 for the HPLC analysis conditions, ESI†). The corresponding fraction was collected and matrix-assisted laser desorption/ionization time-of-flight MS (MALDI-TOF-MS) was performed. As a result, a peak at m/z = 8076.5678 was observed (Fig. 3c), which is almost consistent with the 1 : 1 conjugate of **DBCO-DNA** and **MOC-3** (**MOC-DNA**) (MW = 8086.63. We note that the slight difference may be due to the decomposition of **MOC-3** and adductive cations).[20] Thus, the conjugate was deemed to be successfully formed. Futhermore, neither the peaks derived from the 2 : 1 nor 3 : 1 conjugates of **DBCO-DNA** and **MOC-3** were found (MW = 13610.53, 19133.42, respectively), suggesting the selective formation of a 1 : 1 conjugate (Fig. 3c). In contrast, when the above reaction was performed using **Hexynyl-DNA** instead of **DBCO-DNA**, only a peak derived from unreacted **Hexynyl-DNA** was observed in the MALDI-TOF-MS spectrum (see Fig. S16, ESI†). Thus, it was also proved that the formation of **MOC-DNA** was not facilitated by ionic interactions or coordination of phosphate to the Zr cluster,

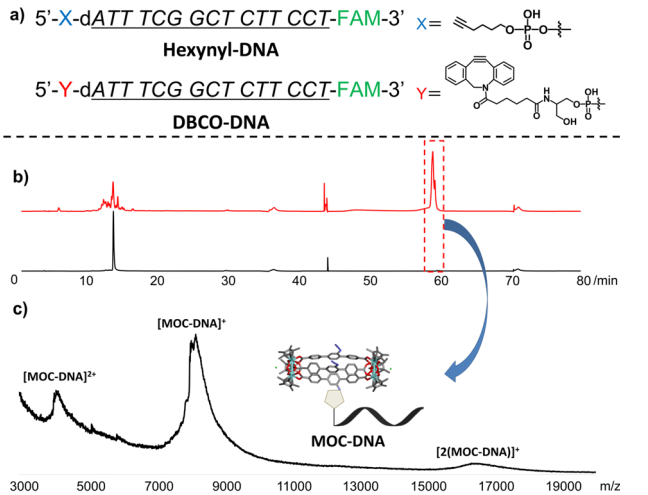

Fig. 3 (a) Structures of **Hexynyl-DNA** and **DBCO-DNA**. (b) HPLC charts. Red: reaction mixture of **MOC-3** and **DBCO-DNA**, black: pure **DBCO-DNA**. (c) MALDI-TOF-MS chart of the fraction collected at around 60 min of the reaction mixture.

but by covalent bond formation between the azide group of **MOC-3** and the alkyne group of **DBCO-DNA**.

Bearing only one DNA strand per cage, **MOC-DNA** has a significant advantage over MOF-DNAs, which have a non-uniform number of DNA molecules, in the design and assembly of higher-order NPMC structures using DNA base pairing. To examine whether **MOC-DNA** can form duplexes, we prepared **Template-DNA** (see Table S1 for the sequence, ESI†) having six repeated units of complementary base sequences. A mixture of **Template-DNA** and **DBCO-DNA** or **MOC-DNA** was heated in a buffer solution (10 mM Tris, pH 7.5, and 75 mM NaCl) at 90 °C for 3 min, then gradually cooled to room temperature (Fig. 4a). The temperature-dependent UV absorbance (λ = 260 nm) was recorded upon heating from 20 to 90 °C for each solution to estimate the ability to form double-strand DNA (dsDNA). A mixture of **Template-DNA** and **DBCO-DNA** showed a sigmoidal temperature-dependent absorbance curve (Fig. S17, ESI†). The sharp increase of UV absorbance at around 70 °C indicates the dissociation of dsDNA, *i.e.*, **Template-DNA** and **DBCO-DNA** mainly exist as dsDNA at room temperature. A mixture of **Template-DNA** and **MOC-DNA** also showed a steep increase of UV absorbance at around 60 °C, indicating their preference for being dsDNA at room temperature (Fig. S17, ESI†). We note that such drastic UV absorbance change was not observed when only one DNA was used (Fig. S18, ESI†).

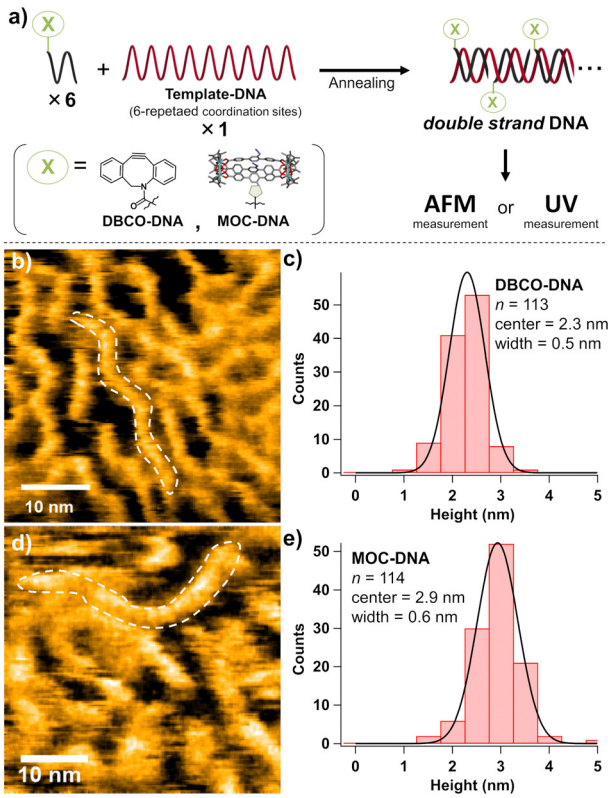

Fig. 4 (a) Scheme of sample preparation for each measurement. HS-AFM images of an annealed sample of **Template-DNA** and (b) **DBCO-DNA** and (d) **MOC-DNA**. The histograms and the Gaussian distributions of the heights of observed objects in an annealed sample of **Template-DNA** and (c) **DBCO-DNA** and (e) **MOC-DNA**. Buffer: 10 mM Tris, pH 7.5, and 75 mM NaCl. The concentration of **Template-DNA** was 0.3 μM and that of **DBCO-DNA** and **MOC-DNA** was 1.8 μM.

Then we tried direct observation of the dsDNA by high-speed atomic force microscopy (HS-AFM) at room temperature. From the HS-AFM image of an annealed mixture of **DBCO-DNA** and **Template-DNA**, string-like objects were observed (Fig. 4b). The objects were roughly 33 nm in length, which agrees with the size expected from the 90 bases of **Template-DNA** (*ca.* 30 nm, see Fig. S19, ESI†). A similar structure was observed in the case of an annealed mixture of **MOC-DNA** and **Template-DNA** (Fig. 4d). Notably, the median height of the structures was 2.9 nm, 0.6 nm higher than in the case of **DBCO-DNA** (Fig. 4c and e). The difference agrees well with the size of the **MOC-3** diameter (~1 nm, Fig. S19, ESI†). The higher feature of the string indicates the presence of MOCs, although the resolution was insufficient to identify their exact position. Overall, **MOC-DNA** can be regularly attached to **Template-DNA** to form dsDNA, demonstrating that the 1 : 1 conjugation of MOC and DNA enabled the one-dimensional arrangement of cages in a nanoscale. Unlike dsDNA, bare **MOC-DNA** was observed as sphere-like structures with string-like materials (Fig. S20, see also ESI† movie), suggesting its aggregation in H_2O. DNA base pairing is essential to construct a controlled assembly of **MOC-DNA**.

The unique 1 : 1 feature of **MOC-DNA** inspired us to explore more of its potential. Because of recent progress in oligonucleotide therapeutics, the intracellular transport of nucleic acids has attained great medical value. However, DNA is polyanionic and hydrophilic, making it difficult to penetrate the negatively charged lipophilic lipid bilayer. Introducing lipophilic substituents into DNA is a promising strategy to enhance the intracellular transport of nucleic acids.[21] Thus, it is curious to investigate whether the modification of lipophilic MOC could accelerate nucleic acid permeation. So we evaluated the cellular uptake of **MOC-DNA** by flow cytometry. HeLa cells were treated with **MOC-DNA** and incubated at 37 °C. Then the cells were washed and fluorescence derived from the FAM moiety (λ_{em} ~ 575 nm) on DNA (Fig. S21, ESI†) was measured. Surprisingly, the mean fluorescence intensity (MFI) of **MOC-DNA**-treated cells gradually increased in a time-dependent manner and almost reached a plateau after 3 h of incubation (Fig. S22, ESI†). Comparing the MFI of cells treated with DNAs for 3 h, the MFI of **MOC-DNA**-treated cells was approximately 8.6-fold higher than that of **DBCO-DNA**-treated cells (Fig. 5a), suggesting that the MOC modification enhanced DNA delivery into the cells. Next, confocal laser scanning microscopy was used to locate the DNA. After treatment with **DBCO-DNA** and washout of free DNA, green fluorescence, which was negligible in the untreated cells, was observed, indicating that the DNA interacted with cells (Fig. 5b and c). However, its distribution seems to be independent of the cell location and it aggregated outside the cells, suggesting that **DBCO-DNA** had quite weak affinity toward the lipid bilayer and could not permeate into the cells.

On the other hand, strong fluorescence was observed at the surface of **MOC-DNA**-treated cells (Fig. 5d) and the fluorescence intensity of the cytoplasm was also obviously higher than that

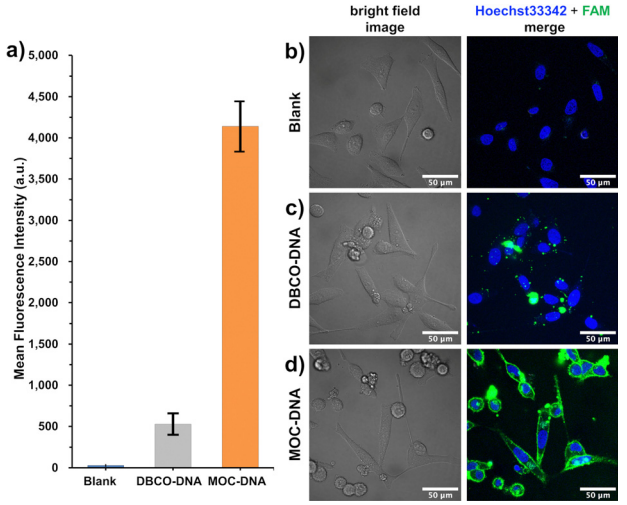

Fig. 5 (a) The cellular uptake of **DBCO-DNA** and **MOC-DNA** measured by flow cytometry. HeLa cells were treated with a 1 μM solution of **DBCO-DNA** or **MOC-DNA**. Error bar represents standard error. Confocal laser scanning microscopy images of HeLa cells treated with (b) only buffer, (c) **DBCO-DNA**, and (d) **MOC-DNA**. The cell nucleus was stained with Hoechst33342. Blue and green colors in merged images represent the nucleus and oligonucleotide, respectively. Scale bars, 50 μm.

of both the untreated cells and **DBCO-DNA**-treated cells (Fig. S23 and S24, ESI†). In addition, there was little correlation between the fluorescence intensity of FAM and Hoechst33342 (Fig. S25, ESI†), showing that **MOC-DNA** that permeated the cell membrane was located more in the cytoplasm than in the nucleus.

We also found that the amount of **MOC-DNA** taken up by HeLa cells was drastically decreased when the cells were incubated at 4 °C (Fig. S26, ESI†), suggesting that **MOC-DNA** was transported into the cells in an energy-dependent manner *via* the proteins on the cell membranes, although the specific pathway is still unclear.

In summary, we synthesized new MOCs having Cp*, which could withstand reactions with DNA. **MOC-3** was successfully conjugated to DNA by a click reaction. The 1 : 1 conjugate of MOC and DNA, **MOC-DNA**, was successfully isolated for the first time. **MOC-DNA** gained the ability to form homogeneous duplexes, which will facilitate the creation of programmed NPMC assemblies using the structural designability of DNA. Furthermore, **MOC-DNA** dramatically improved the cell permeability of DNA compared with bare DNA. Thus, MOCs can be a quantitative and simultaneous transporter of DNA and drug molecules, with great potential for medical applications. We demonstrated that conjugating discrete NPMC with DNA offers both materials and biological applications. Although the pore size of MOCs demonstrated here is not large enough, we are convinced that this study will be a milestone in exploring the integrated function of guest-included NPMC and DNA.

This work was supported by the PRESTO (JPMJPR141C), CREST (JPMJCR17I3) and COI-NEXT (JPMJPF2204) of the Japan Science and Technology Agency (JST), AMED (JP19am0401008), JSPS KAKENHI Grant Numbers JP19H02734, JP20K20564, JP21J15463, JP22K05141, JP22H00324, JP21K14750, and Canon Medical Systems Corporation. ''Graduate Program of Transformative Chem-Bio Research'' in Nagoya University, supported by MEXT (WISE Program) is also acknowledged.

Conflicts of interest

There are no conflicts to declare.

Notes and references

1 B. S. Pilgrim and N. R. Champness, *ChemPlusChem*, 2020, **85**, 1842–1856.
2 H. Miura, V. Bon, I. Senkovska, S. Ehrling, N. Bönisch, G. Mäder, S. Grünzner, A. Khadiev, D. Novikov, K. Maity, A. Richter and S. Kaskel, *Adv. Mater.*, 2022, **2207741**, 2207741.
3 G. R. Lorzing, B. A. Trump, C. M. Brown and E. D. Bloch, *Chem. Mater.*, 2017, **29**, 8583–8587.
4 R. A. Perlata, M. T. Huxley, Z. Shi, Y. B. Zhang, C. J. Sumby and C. J. Doonan, *Chem. Commun.*, 2020, **56**, 15313–15316.
5 A. C. Ghosh, A. Legrand, R. Rajapaksha, G. A. Craig, C. Sassoye, G. Balázs, D. Farrusseng, S. Furukawa, J. Canivet and F. M. Wisser, *J. Am. Chem. Soc.*, 2022, **144**, 3626–3636.
6 S. Karmakar, S. Barman, F. A. Rahimi and T. K. Maji, *Energy Environ. Sci.*, 2021, **14**, 2429–2440.
7 S. Haddad, I. Abánades Lázaro, M. Fantham, A. Mishra, J. Silvestre-Albero, J. W. M. Osterrieth, G. S. Kaminski Schierle, C. F. Kaminski, R. S. Forgan and D. Fairen-Jimenez, *J. Am. Chem. Soc.*, 2020, **142**, 6661–6674.
8 W. Zhu, J. Guo, Y. Ju, R. E. Serda, J. G. Croissant, J. Shang, E. Coker, J. O. Agola, Q. Z. Zhong, Y. Ping, F. Caruso and C. J. Brinker, *Adv. Mater.*, 2019, **31**, 1806774.
9 M. Kalaj and S. M. Cohen, *Angew. Chem., Int. Ed.*, 2020, **59**, 13984–13989.
10 X. Y. Xie, F. Wu, X. Liu, W. Q. Tao, Y. Jiang, X. Q. Liu and L. B. Sun, *Chem. Commun.*, 2019, **55**, 6177–6180.
11 X. Yang, J. Lv, Z. Yang, R. Yuan and Y. Chai, *Anal. Chem.*, 2017, **89**, 11636–11640.
12 G. Zhang, D. Shan, H. Dong, S. Cosnier, K. A. Al-Ghanim, Z. Ahmad, S. Mahboob and X. Zhang, *Anal. Chem.*, 2018, **90**, 12284–12291.
13 W. Ning, Z. Di, Y. Yu, P. Zeng, C. Di, D. Chen, X. Kong, G. Nie, Y. Zhao and L. Li, *Small*, 2018, **14**, 1703812.
14 P. Zhang, Y. Ouyang, Y. S. Sohn, R. Nechushtai, E. Pikarsky, C. Fan and I. Willner, *ACS Nano*, 2021, **15**, 6645–6657.
15 G. Yao, F. Zhang, F. Wang, T. Peng, H. Liu, E. Poppleton, P. Šulc, S. Jiang, L. Liu, C. Gong, X. Jing, X. Liu, L. Wang, Y. Liu, C. Fan and H. Yan, *Nat. Chem.*, 2020, **12**, 1067–1075.
16 S. Wang, C. M. McGuirk, M. B. Ross, S. Wang, P. Chen, H. Xing, Y. Liu and C. A. Mirkin, *J. Am. Chem. Soc.*, 2017, **139**, 9827–9830.
17 S. Wang, S. S. Park, C. T. Buru, H. Lin, P. C. Chen, E. W. Roth, O. K. Farha and C. A. Mirkin, *Nat. Commun.*, 2020, **11**, 1–8.
18 A. Carné-Sánchez, J. Albalad, T. Grancha, I. Imaz, J. Juanhuix, P. Larpent, S. Furukawa and D. Maspoch, *J. Am. Chem. Soc.*, 2019, **141**, 4094–4102.
19 G. Liu, Y. Di Yuan, J. Wang, Y. Cheng, S. B. Peh, Y. Wang, Y. Qian, J. Dong, D. Yuan and D. Zhao, *J. Am. Chem. Soc.*, 2018, **140**, 6231–6234.
20 J. Albalad, A. Carné-Sánchez, T. Grancha, L. Hernández-López and D. Maspoch, *Chem. Commun.*, 2019, **55**, 12785–12788.
21 C. Wolfrum, S. Shi, K. N. Jayaprakash, M. Jayaraman, G. Wang, R. K. Pandey, K. G. Rajeev, T. Nakayama, K. Charrise, E. M. Ndungo, T. Zimmermann, V. Koteliansky, M. Manoharan and M. Stoffel, *Nat. Biotechnol.*, 2007, **25**, 1149–1157.